CrossMark

J. Fluid Mech. (2015), *vol.* 784, *pp.* 51–73. © Cambridge University Press 2015
doi:10.1017/jfm.2015.578

Third-order resonant wave interactions under the influence of background current fields

Takuji Waseda[1,†], T. Kinoshita[2], L. Cavaleri[3] and A. Toffoli[4]

[1]Graduate School of Frontier Sciences, University of Tokyo, Kashiwa, Chiba 277-8563, Japan

[2]Institute of Industrial Science, University of Tokyo, Tokyo 153-8505, Japan

[3]Institute of Marine Sciences, Castello 2737/F, 30122 Venice, Italy

[4]Centre for Ocean Engineering, Science and Technology, Swinburne University of Technology, P.O. Box 218, Hawthorn, Victoria 3122, Australia

(Received 10 October 2014; revised 4 August 2015; accepted 28 September 2015; first published online 29 October 2015)

A series of experiments were conducted in a wave basin (50 m long, 10 m wide and 5 m deep) generating two waves propagating at an angle by a directional wavemaker. When the two waves were selected from a resonant triplet, an initially non-existing wave grew as the waves propagated down the tank. The linear growth rate of the resonating wave agreed well with third-order resonance theory based on Zakharov's reduced gravity equation. Additional experiments with opposing and coflowing mean current with large temporal and spatial variations were conducted. As the flow rate increased, the linear growth was suppressed. As reproduced numerically with Zakharov's equation, the resonant interaction saturated at time scales inversely proportional to the magnitude of the forced random resonance detuning. It is conjectured that the resonance is detuned by the variation and not by the mean of the current field due to wavelength-dependent Doppler shift and to the refraction of wave rays. Further analysis of the spectral evolution revealed that while discrete peaks appear at high frequencies as a result of dynamical cascading, a continuously saturated spectrum develops in the background as the current speed increases. Additional experiments were conducted studying the evolution of the random directional wave on a dynamical time scale under the influence of current. Due to random resonance detuning by the current, the spectral tail tended to be suppressed.

Key words: surface gravity waves, waves/free-surface flows

1. Introduction

The fundamental theories of the evolution of ocean waves were established in the 1950s and 1960s. Ocean waves are generated due to the wind and its self-similar wave spectrum downshifts due to nonlinear wave–wave interaction (Miles 1957; Phillips 1958; Hasselmann 1962). Numerous works extending these theories were developed over the years. They are now implemented in wave forecasting models, but empiricism is to a certain degree unavoidable (Cavaleri *et al.* 2007). The heart of

† Email address for correspondence: waseda@k.u-tokyo.ac.jp

https://doi.org/10.1017/jfm.2015.578 Published online by Cambridge University Press

the so-called third generation wave model is the four-wave resonance that was first described by Phillips (1960) as a deterministic process and by Hasselmann (1962) as a stochastic process. Zakharov (1968) independently derived an integro-differential equation of wave evolution for spectral components and showed that Hasselman's solution can be rederived by randomising the wave field.

Surprisingly, however, studies validating the four-wave resonance are rather limited. Historical experiments were conducted independently, but almost simultaneously, by Longuet-Higgins & Smith (1966) and McGoldrick *et al.* (1966) using a rectangular wave basin with wavemakers at two sides generating two waves crossing at 90°. A third wave will grow in space as a result of four-wave interaction in which one of the waves is counted twice. The growth rate of the third wave agrees with the theory of tertiary wave interaction. Tomita (1989) conducted a similar experiment and showed that the third wave will evolve in both space and time. Alternatively, experimental verification of the theory of four-wave resonance is possible by estimating the initial growth rate of the Benjamin–Feir instability (e.g. Tulin & Waseda 1999).

Based on these earlier works, it is in general conceived that waves of infinitesimal amplitude satisfying the linear dispersion relationship will form a resonant quartet in deep water and a resonant triad in shallower water. Further extension of resonance theory to include the finite amplitude effect was made, for example, by Madsen & Fuhrman (2006). The so-called Phillips figure of eight diagram, representing the resonance manifold, is modified as a result of amplitude dispersion. An interesting consequence of the finite amplitude resonance condition is the existence of resonant progressive short-crested waves of permanent form (Hammack, Henderson & Segur 2005; Xu *et al.* 2012; Liu & Liao 2014). Liao (2011) theoretically derived a solution corresponding to this permanent short-crested wave by means of a homotopy analysis method, and later Xu *et al.* (2012) showed that the derivation is consistent with Zakharov's theory. Experimental validation of this permanent wave form was conducted recently by Liu *et al.* (2015) in a sizeable square basin. Not a lot of study has been conducted yet on unsteady nonlinear resonant waves, but it should be recalled that the instability of Stokes waves is indeed a consequence of the cancellation of resonance detuning by amplitude dispersion.

Numerical validations have been conducted in both the periodic domain and the non-periodic domain. Unlike most physical experiments in a wave basin, where waves are left to evolve only in space, the numerical test can be made with a periodic boundary condition in space. We can then observe the growth of waves in time. The limitation of this approach is that the allowable wavenumber will be quantised, and, therefore, the exact resonance condition cannot be achieved (e.g. Hirobe 2013; W. Choi, personal communication, 2012). Fuhrman, Madsen & Bingham (2006) have implemented a Boussinesq-type model in a non-periodic rectangular domain including wave generating and absorbing regions at both ends of the domain with reflecting side boundaries, thus reproducing waves in a domain similar to a narrow flume. Short-crested instability was studied and it was successfully demonstrated that resonance quartet interaction can occur in a closed basin.

Indirectly, the consequence of four-wave interaction can be validated, observing the nonlinear transfer function of the random directional wave. However, the required kinetic time scale necessary for the establishment of Hasselman's interaction is much longer than the time scale of laboratory experiments (e.g. Janssen 2003). Tanaka (2001) has conducted an extensive numerical simulation of a fully nonlinear model and showed that a Hasselman-like transfer function can be reproduced on a dynamical time scale. Moreover, even on a dynamical time scale, an equilibrium

https://doi.org/10.1017/jfm.2015.578 Published online by Cambridge University Press

tail seems to develop (Waseda, Kinoshita & Tamura 2009). They have shown that an equilibrium tail can develop in a narrow channel, and the exponent of the tail depends on the directional spreading. It should be noted that in both fully nonlinear numerical simulations and tank experiments, the wavenumber spectrum is discretised and, therefore, exact resonances cannot occur. The nonlinear energy transfer occurs on a much faster time scale among a detuned quartet of waves.

The effect of a background current on the resonance has been studied for the degenerate case of modulational instability of a Stokes wave, which plays a pivotal role in freak wave generation, by Toffoli *et al.* (2013, 2015). They have experimentally confirmed the foresight of Onorato, Proment & Toffoli (2011), who have shown that the generation of rogue waves is triggered when waves enter a field of opposing current. Onorato *et al.* (2011) made use of the current-modified nonlinear Schrödinger equation derived by Hjelmervik & Trulsen (2009). Under the influence of a random current field, linear focusing effects can enhance the generation of freak waves (White & Fornberg 1998), and this is further strengthened by an opposing current field (Wu & Yao 2004). Hjelmervik & Trulsen (2009) investigated the effect of nonlinearity on the linear refraction effect, and showed that depending on the current and wave, the probability of freak waves can either grow or decrease when the wave height increases due to linear refraction. Although these phenomena are related to resonant interaction of waves, it is not necessarily apparent how the exact resonance can be affected when a background current field is present.

In this study, we will first explore experimentally the validity of the four-wave interaction in a narrow channel. The experimental evolution of the resonant wave system will be compared with the growth rate based on Zakharov's theory (Zakharov 1968) augmented by Krasitskii (1994). For the case of a DIA (discrete interaction approximation) quartet, a background current field will be added. The resulting suppression of the resonant interaction will be numerically investigated, introducing constant and random resonant detuning. A possible consequence of the random detuning suppressing the resonance will be studied experimentally by the evolution of the irregular directional wave. Dynamical cascade among free and bound waves will be discussed as well. In § 2, the theoretical basis of the resonant interaction of tertiary waves is given. The facility and experimental conditions of the cases presented in this paper, together with the description of the current field with large variations, are presented in § 3. Experimental results for the resonant wave systems are given in § 4. The discussion section contains the result of the numerical solution and additional experiments on the irregular directional spectrum, § 5. The conclusion follows.

2. Theoretical basis

The evolution of nonlinear surface waves interacting with each other is studied on the basis of the Zakharov equation (Zakharov 1968). The kernels of the interaction and the necessary canonical transformation are described in Krasitskii (1994). The four-wave reduced equation for a pure gravity wave reads

$$\mathrm{i}\frac{\partial b_0}{\partial t} = \omega_0 b_0 + \int \tilde{V}_{0123} b_1^* b_2 b_3 \delta_{0+1-2-3}\,\mathrm{d}k_{123}, \tag{2.1}$$

where the canonical variables b_i are related to the Fourier coefficients of the surface elevation and surface potential through a cumbersome canonical transformation. The interaction coefficient $\tilde{V}_{0,1,2,3}$ is determined by the wavenumber vectors $\boldsymbol{k}_0, \boldsymbol{k}_1, \boldsymbol{k}_2, \boldsymbol{k}_3$

https://doi.org/10.1017/jfm.2015.578 Published online by Cambridge University Press

and the $\delta_{0+1-2-3} = \delta(\boldsymbol{k}_0 + \boldsymbol{k}_1 - \boldsymbol{k}_2 - \boldsymbol{k}_3)$. The details are given in the original paper by Krasitskii (1994) or an illuminating text book by Janssen (2004). By introducing a discrete spectrum, an integro-differential equation can be expressed as a summation of discrete interaction terms:

$$\mathrm{i}\frac{\partial b_0}{\partial t} = \omega_0 b_0 + \sum_{0+1-2-3} T_{0123} b_1^* b_2 b_3, \tag{2.2}$$

where $T_{0,1,2,3}$ represents the interaction coefficient $\tilde{V}_{0,1,2,3}$ evaluated at each four-wave combination. In this study, we investigate the interaction of a set of four waves (b_1, b_2, b_3, b_4) exactly in resonance or slightly off of the resonance condition,

$$\left.\begin{array}{c} \omega_1 + \omega_2 = \omega_3 + \omega_4 + \Delta_{1234}, \\ \boldsymbol{k}_1 + \boldsymbol{k}_2 = \boldsymbol{k}_3 + \boldsymbol{k}_4. \end{array}\right\} \tag{2.3}$$

The wave frequency ω and the wavenumber vector $\boldsymbol{k}$ satisfies the linear dispersion relationship of surface gravity waves, $\omega^2 = gk\tanh(kh)$, where $k = |\boldsymbol{k}|$ and h is the depth. In the following, the depth is assumed to be infinite. A straightforward comparison of the theory with a physical experiment on four-wave interaction is not possible because of the use of the canonical variable and the canonical transformation. Retaining only the linear term of the canonical transformation $a_0 = b_0 + N.L.T.$ and assuming linear surface elevation and velocity potential at the free surface, i.e. $\zeta(\boldsymbol{k}) = \mathrm{i}(|\boldsymbol{k}|/\omega(|\boldsymbol{k}|))\psi(\boldsymbol{k})$, we obtain the following relationship which relates the observed surface elevation to the canonical variables in (2.2):

$$b(\boldsymbol{k}) = \zeta(\boldsymbol{k})\left[\frac{\omega(|\boldsymbol{k}|)}{2|\boldsymbol{k}|}\right]^{1/2} + \mathrm{i}\psi(\boldsymbol{k})\left[\frac{|\boldsymbol{k}|}{2\omega(|\boldsymbol{k}|)}\right]^{1/2} \approx 2c_g^{1/2}\zeta(\boldsymbol{k}), \tag{2.4}$$

where $\zeta(\boldsymbol{k}) = \zeta^*(-\boldsymbol{k})$ and $\psi(\boldsymbol{k}) = \psi^*(-\boldsymbol{k})$ are respectively the Fourier coefficients of the free-surface elevation and velocity potential at the free surface, and $c_g = (\omega(|\boldsymbol{k}|)/2|\boldsymbol{k}|)$ is the group velocity. By applying the change of variables $\zeta_i(\boldsymbol{k}_i, t) = \hat{\zeta}_i(\boldsymbol{k}_i)\exp(-\mathrm{i}\omega_i t)$, we obtain the evolution equation of free-surface wave amplitudes, evaluated with physical variables, $\hat{\zeta} = |\hat{\zeta}|\mathrm{e}^{-\mathrm{i}\theta} = a\mathrm{e}^{-\mathrm{i}\theta}/2$ and $\eta = a\cos\theta = \hat{\zeta} + \hat{\zeta}^* = 2|\hat{\zeta}|\cos\theta$,

$$\frac{\partial a_0}{\partial t} = \sum_{0+1-2-3}\left(\frac{c_{g1}c_{g2}c_{g3}}{c_{g0}}\right)^{1/2} T_{0123}a_1a_2a_3\sin(\Theta_{0123} + \Delta_{0123}t), \tag{2.5a}$$

$$\frac{\partial \theta_0}{\partial t} = \sum_{0+1-2-3}\left(\frac{c_{g1}c_{g2}c_{g3}}{c_{g0}}\right)^{1/2} T_{0123}\frac{a_1a_2a_3}{a_0}\cos(\Theta_{0123} + \Delta_{0123}t), \tag{2.5b}$$

where $\Theta_{0123} = \theta_0 + \theta_1 - \theta_2 - \theta_3$.

The evolution equation for the quasi-resonant or near-resonant quartet, equivalent to Benney's equation (Benney 1962), can be obtained:

$$\frac{\partial a_0}{\partial t} = 2T_{0123}\left(\frac{c_{g1}c_{g2}c_{g3}}{c_{g0}}\right)^{1/2} a_1a_2a_3\sin(\Theta_{0123} + \Delta_{0123}t), \tag{2.6a}$$

$$\begin{aligned}\frac{\partial \theta_0}{\partial t} &= \left(T_{0000}c_{g0}a_0^2 + 2T_{0101}c_{g1}a_1^2 + 2T_{0202}c_{g2}a_2^2 + 2T_{0303}C_{g3}a_3^2\right) \\ &\quad + 2T_{0123}\left(\frac{c_{g1}c_{g2}c_{g3}}{c_{g0}}\right)^{1/2}\frac{a_1a_2a_3}{a_4}\cos(\Theta_{0123} + \Delta_{0123}t).\end{aligned} \tag{2.6b}$$

https://doi.org/10.1017/jfm.2015.578 Published online by Cambridge University Press

A variety of evolution equations can be derived from (2.6*a*,*b*). The evolution equation for the initially infinitesimal fourth wave, when the exact resonance condition $\Delta_{1234} = 0$ is satisfied, reads

$$\frac{\partial a_4}{\partial t} = 2T_{1234}\left(\frac{c_{g1}c_{g2}c_{g3}}{c_{g4}}\right)^{1/2} a_1 a_2 a_3 \sin\Theta_{1234}, \tag{2.7a}$$

$$\frac{\partial \theta_4}{\partial t} = (2T_{1414}c_{g1}a_1^2 + 2T_{2424}c_{g2}a_2^2 + 2T_{3434}C_{g3}a_3^2) + 2T_{1234}\left(\frac{c_{g1}c_{g2}c_{g3}}{c_{g4}}\right)^{1/2} \frac{a_1 a_2 a_3}{a_4}\cos\Theta_{1234}. \tag{2.7b}$$

Equation (2.7*a*) holds as long as the condition $|a_1|, |a_2|, |a_3| \gg |a_4|$ is satisfied. The amplitude of the three waves does not change, and only the fourth wave will grow at the expense of the energy of the other three waves. The growth of the fourth wave is largest when $\sin(\Theta_{1+2-3-4}) = 1$. We may then expect that the phase of the fourth wave should satisfy $\theta_4 = \theta_1 + \theta_2 - \theta_3 - \pi/2$ for the fastest growing resonant wave. A small difference from this condition will lead to a rapid change of the phase θ_4 because of the singularity when a_4 is infinitesimal.

To the order of approximation (2.7*a*), the rate of growth of the fourth wave is estimated to be

$$\alpha_t = 2T_{1234}\left(\frac{c_{g1}c_{g2}c_{g3}}{c_{g4}}\right)^{1/2} a_1 a_2 a_3. \tag{2.8}$$

The fourth wave will grow linearly in time, $a_4 = \alpha_t t$. It is convenient to apply a coordinate transformation $x = c_{g4}t$ for the fourth wave. When the wave is propagating at an angle ϕ_4 to the coordinate x, the linear growth rate in space along x can be approximated as

$$\alpha_x = 2\frac{\cos\phi_4}{c_{g4}} T_{1234}\left(\frac{c_{g1}c_{g2}c_{g3}}{c_{g4}}\right)^{1/2} a_1 a_2 a_3. \tag{2.9}$$

This expression for the growth rate is convenient when comparing the experimental estimate with the theory.

The evolution equation for the tertiary wave interaction can be obtained:

$$\left.\begin{aligned} 2\omega_1 &= \omega_2 + \omega_3, \\ 2\boldsymbol{k}_1 &= \boldsymbol{k}_2 + \boldsymbol{k}_3. \end{aligned}\right\} \tag{2.10}$$

Assuming that the initial amplitude of the third wave is infinitesimal, the linearised evolution equation for the third wave can be derived from (2.5*a*):

$$\frac{\partial a_3}{\partial t} = T_{2311}\left(\frac{c_{g2}c_{g1}^2}{c_{g3}}\right)^{1/2} a_1^2 a_2 \sin\Theta_{2311}, \tag{2.11a}$$

$$\frac{\partial \theta_3}{\partial t} = \left(2T_{1313}c_{g1}a_1^2 + 2T_{2323}C_{g2}a_2^2\right) + T_{2311}\left(\frac{c_{g1}^2 c_{g2}}{c_{g3}}\right)^{1/2} \frac{a_1^2 a_2}{a_3}\cos\Theta_{2311}. \tag{2.11b}$$

https://doi.org/10.1017/jfm.2015.578 Published online by Cambridge University Press

The corresponding linear growth rates in time and space are

$$\alpha_t = T_{2311}\left(\frac{c_{g1}^2 c_{g2}}{c_{g3}}\right)^{1/2} a_1^2 a_2, \tag{2.12a}$$

$$\alpha_x = \frac{\cos\phi_3}{c_{g3}} T_{2311}\left(\frac{c_{g1}^2 c_{g2}}{c_{g3}}\right)^{1/2} a_1^2 a_2. \tag{2.12b}$$

3. Facility and experimental conditions

3.1. *Facility*

The experiment was conducted at the Ocean Engineering Basin of the Institute of Industrial Science, the University of Tokyo (Kinoshita Lab/Rheem Lab). The dimension of the tank is 50 m in length, 10 m in width and 5 m in depth. The wavemaker is located at one end of the tank with 32 plungers controlled independently. Typically, an array of wave-wire gauges are placed at 5 m intervals 2.5 m away from the side wall to monitor the evolution of the wave along the tank (see, e.g., Waseda *et al.* 2009). The entire volume of the tank water can be circulated in both directions, coflowing and opposing the wave propagation direction. The inlet and outlet of the water are located beneath the wavemaker and the beach (figure 1). The inlet is 3.5 m high and 10 m wide, the outlet 3.0 and 10 m. The inlet consists of two rows of screens, and 1.85 m long vertical guide walls placed at one metre intervals. The outlet has only one screen, and the vertical guide walls are 1.0 m long. The water enters into or exits from a 3 m diameter pipe at the side. Therefore, the flow makes an abrupt 90° turn behind the guide walls under the wavemaker and beneath the beach. Because of this configuration, the mean current field is not uniform across the tank and has a vertical shear as well (figure 1 and also Toffoli *et al.* 2013, 2015). The coflowing current is better regulated than the opposite condition because of the different inlet and outlet configurations. The waves refract as they enter into a sheared current field (see figure 1*b*). At times, the refraction is strong enough to be recognised visually.

3.2. *Experimental conditions*

Experimental validations of the third-order resonant wave interactions have been conducted mostly in rectangular basins with wavemakers capable of generating waves at 90° angle (Longuet-Higgins & Smith 1966; McGoldrick *et al.* 1966; Tomita 1989). The so-called tertiary wave interaction (Longuet-Higgins 1962) is a special case of the four-wave interaction where the primary wave (f_1) is counted twice to satisfy the exact resonance condition, with the longer wave normal to the primary wave (f_2) and the third wave (f_3) propagating at 9.4° to f_1. Their frequencies ω, wavenumbers $\boldsymbol{k}$ and propagating directions ϕ satisfy the following conditions:

$$\left.\begin{array}{r} 2\omega_1 = \omega_2 + \omega_3, \\ 2\boldsymbol{k}_1 = \boldsymbol{k}_2 + \boldsymbol{k}_3, \end{array}\right\} \quad \left.\begin{array}{c} \omega_1 = 1.7356\omega_2, \\ |k_1| = 3.0113|k_2|, \end{array}\right\} \quad \left.\begin{array}{c} \phi_1 = 0, \\ \phi_2 - \phi_1 = -90, \\ \phi_3 - \phi_1 = +9.4. \end{array}\right\} \tag{3.1a–c}$$

Apparently, such an experiment cannot be conducted in a narrow flume. However, it is possible to generate f_1 and f_3, and let f_2 naturally emerge and propagate across the

https://doi.org/10.1017/jfm.2015.578 Published online by Cambridge University Press

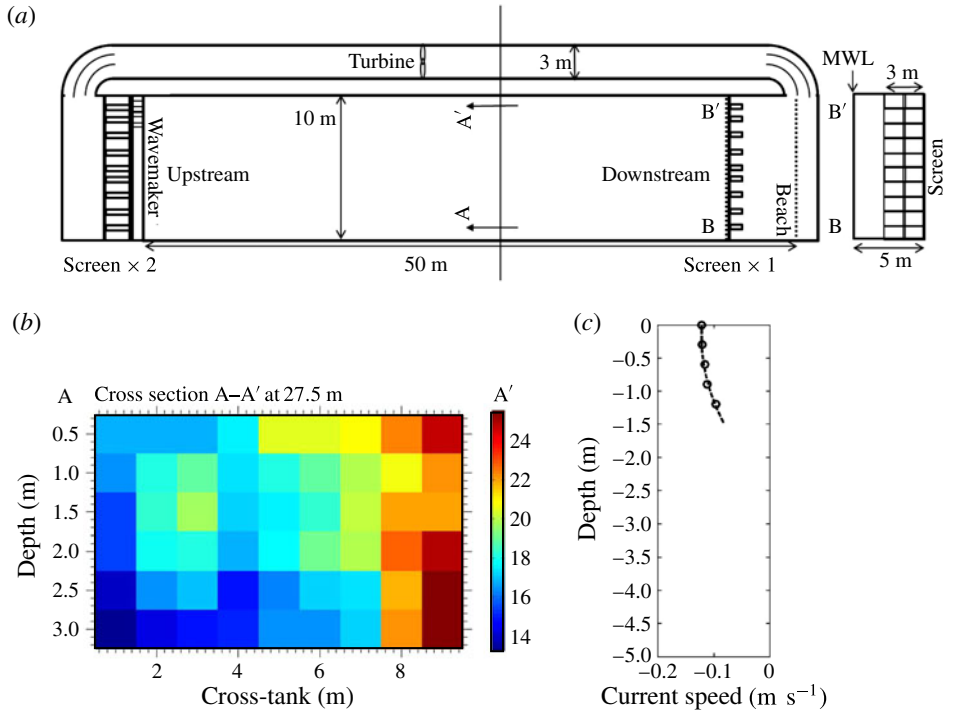

FIGURE 1. Description of the Ocean Engineering Basin of the Institute of Industrial Sciences, the University of Tokyo. (*a*) Plan view of the tank showing the configuration of the water circulation system. (*b*) Vertical section of the current speed for a case with strong mean current (over 20 cm s^{-1}). It should be noted that this case was not used for the experiments in this study. (*c*) Vertical velocity profile for a case of surface mean current around 12 cm s^{-1}.

tank. The first test case (case 1, see table 1) was designed such that the wavelength of the secondary wave was 2/3 of the tank width, so that the sloshing wave mode would be excited. Making use of the sloshing condition gives an advantage for the easy detection of the emergence of the initially non-existing resonant wave. As a comparison, an off-resonant wave system was generated as well, retaining the frequency of f_3 but changing the propagation angle to be 20° to the primary wave (case 2).

The discrete interaction approximation (DIA, Hasselmann & Hasselmann 1985) greatly simplifies the collision integral of the nonlinear wave interaction by selecting just one combination of the quartet from the set of infinite combinations. The DIA quadruplet consists of three waves that satisfy the exact resonance condition:

$$\left.\begin{aligned} 2\omega_1 &= \omega_2 + \omega_3, \\ 2\boldsymbol{k}_1 &= \boldsymbol{k}_2 + \boldsymbol{k}_3, \end{aligned}\right\} \quad \left.\begin{aligned} \omega_2 &= (1-0.25)\,\omega_1, \\ \omega_3 &= (1+0.25)\,\omega_1, \end{aligned}\right\} \quad \left.\begin{aligned} \phi_1 &= 0, \\ \phi_2 - \phi_1 &= -33.6, \\ \phi_3 - \phi_1 &= +11.5. \end{aligned}\right\} \qquad (3.2a\text{–}c)$$

Among the three waves, the primary wave that propagates along the tank (f_1) and the secondary wave (f_2) that propagates at 33.6° were generated (case 3, table 1). The primary wave was 0.91 m, the secondary wave 1.6 m and the tertiary wave

https://doi.org/10.1017/jfm.2015.578 Published online by Cambridge University Press

https://doi.org/10.1017/jfm.2015.578 Published online by Cambridge University Press

Case	Waves	f (Hz)	ω (rad s^{-1})	k (rad m^{-1})	λ (m)	ak	ϕ (deg.)	kh	U (cm s^{-1})	U_{dop} (cm s^{-1})	kU_{dop} (rad s^{-1})	Δ_{kU} (rad s^{-1})
1 Tertiary	f_1	0.84	5.28	2.86	2.2	0.029	0	14.3	—	—	—	—
	f_2, f_2'	0.484	3.04	0.94	6.67	—	±90	4.7	—	—	—	
	f_3, f_3'	1.2	7.54	5.76	1.09	0.058	∓9.4	28.8	—	—	—	
2 Off-resonant	f_1	0.84	5.28	2.86	2.2	0.029	0	14.3	—	—	—	
	f_2, f_2'	—	—	—	—	—	—	—	—	—	—	
	f_3, f_3'	1.2	7.54	5.76	1.09	0.058	∓20	28.8	—	—	—	
3 DIA	f_1	1.31	8.23	6.9	0.91	0.055	0	34.5	—	—	—	—
	f_2, f_2'	0.988	6.21	3.93	1.6	0.022	∓33.6	19.7	—	—	—	
	f_3, f_3'	1.64	10.3	10.8	0.58	—	±11.5	54.0	—	—	—	
4 DIA off-resonant	f_1	1.31	8.23	6.9	0.91	0.055	0	34.5	—	—	—	—
	f_2, f_2'	0.988	6.21	3.93	1.6	0.022	∓20.0	19.7	—	—	—	
	f_3, f_3'	1.64	10.3	10.8	0.58	—	—	54.0	—	—	—	
5 DIA	f_1	1.31	8.23	6.9	0.91	0.055	0	34.5	−8.32	−8.33	−0.575	−0.00282
	f_2, f_2'	0.988	0.988	3.93	1.6	0.022	∓33.6	19.7		−8.24	−0.270	
−8.32 cm s^{-1}	f_3, f_3'	1.64	10.3	10.8	0.58	—	±11.5	54.0		−8.34	−0.883	
6 DIA	f_1	1.31	8.23	6.9	0.91	0.055	0	34.5	−5.41	−5.41	−0.373	−0.00248
	f_2, f_2'	0.988	0.988	3.93	1.6	0.022	∓33.6	19.7		−5.36	−0.175	
−5.41 cm s^{-1}	f_3, f_3'	1.64	10.3	10.8	0.58	—	±11.5	54.0		−5.42	−0.574	
7 DIA	f_1	1.31	8.23	6.9	0.91	0.055	0	34.5	−3.82	−3.82	−0.264	−0.00224
	f_2, f_2'	0.988	0.988	3.93	1.6	0.022	∓33.6	19.7		−3.79	−0.124	
−3.82 cm s^{-1}	f_3, f_3'	1.64	10.3	10.8	0.58	—	±11.5	54.0		−3.83	−0.405	
8 DIA	f_1	1.31	8.23	6.9	0.91	0.055	0	34.5	7.41	7.42	0.512	0.00264
	f_2, f_2'	0.988	0.988	3.93	1.6	0.022	∓33.6	19.7		7.34	0.240	
7.41 cm s^{-1}	f_3, f_3'	1.64	10.3	10.8	0.58	—	±11.5	54.0		4.3	0.786	
9 DIA	f_1	1.31	8.23	6.9	0.91	0.055	0	34.5	0.89	0.89	0.061	0.00018
	f_2, f_2'	0.988	0.988	3.93	1.6	0.022	∓33.6	19.7		0.88	0.029	
0.89 cm s^{-1}	f_3, f_3'	1.64	10.3	10.8	0.58	—	±11.5	54.0		0.89	0.094	

TABLE 1. Wave parameters for the quartet experiments. f is the frequency, ω is the angular frequency, k is the wavenumber, λ is the wavelength, ak is the steepness, ϕ is the initial phase, and kh is the non-dimensional depth. U is the mean background current field. U_{dop} is the effective Doppler speed, and kU_{dop} is the frequency shift. Δ_{kU} is the resonance detuning due to background current field.

0.58 m long. The initial steepnesses were 0.055 and 0.022 for the primary and secondary waves. The cross-tank wavenumbers (k_y) did not match the integer division of twice the tank width ($20/n$ m or $0.314n$ rad m^{-1}, where $n = 1, 2, 3, \ldots$), and, therefore, the cross-wave (or the sloshing wave) studied by Jones (1984), Kit, Shemer & Miloh (1987) and Yao, Tulin & Kolaini (1994), or the oblique waves studied by Trulsen, Stansberg & Velarde (1999) were not excited directly. As a comparison, the off-resonant case was tested as well. Retaining the frequency, the angle of the secondary wave was changed to $-20°$ (case 4). In this case the primary and the secondary waves alone cannot resonate to generate the third wave.

It should be noted that to take advantage of the symmetry of the sidewall reflections, we actually generated waves propagating at both positive and negative angles for all of the experimental cases. It is known for irregular waves that the statistical properties of the random waves are more homogeneous in a narrow channel than in a rectangular basin with two wavemakers at normal angle (Takezawa, Kobayashi & Kasahara 1988). Indeed, the sidewall reflections fill in the diffraction region as described by Dalrymple (1989). Those additional waves are denoted as f_i' in table 1.

The values of kh for the waves used in the experiments, where k is the wavenumber and $h = 5$ m is the depth, were 14.3, 4.7 and 28.8 for the tertiary wave case and 34.5, 19.7 and 54.0 for the DIA case. Therefore, all of the experimental cases can be considered to be in deep water conditions, where the depth effect can be neglected.

For the DIA condition (case 3), background currents were added. Three cases of the opposing mean current (case 5, -8.32 cm s^{-1}; case 6, -5.39 cm s^{-1}; case 7, -3.71 cm s^{-1}), and two cases of the coflowing mean current cases (case 8, 7.41 cm s^{-1}; case 9, 0.89 cm s^{-1}) were tested. The associated Doppler Speed U_{dop}, frequency shift kU_{dop} and resonance detuning Δ_{kU} are listed as well. These will be explained in § 4.2.

3.3. *Current field in the tank*

The mean current field has large horizontal and vertical gradients because of the geometry of the circulation system (figure 1*a*). The current tends to be stronger on the side where the orifices of the pipes are located, because the flow makes an abrupt 90° turn and cannot diffuse across the tank (figure 1*b*). The inlet and outlet are located near the bottom of the tank (3.5 m and 3.0 m high, 10 m wide) and occupy 60–70 % of the entire vertical section. The flow needs to diverge at the inlet and converge at the outlet. Therefore, the vertical profile is likely to vary along the tank. From the measurement taken at approximately 20 m from the wavemaker, the velocity decays with depth down to 1.2 m (figure 1*c*). With a vertical shear, the Doppler speed depends on the wavenumber.

Furthermore, the current speed is highly variable. The time records of an electro-magnetic current meter located at 10 m (solid line) and 20 m (thick solid line) from the wavemaker are shown in figure 2 for cases 5–9, i.e. for the average current speeds of -7.79, -5.39, -3.71, 0, 0.89 and 7.41 cm s^{-1}. For example, at the highest opposing current speed case (-7.79 cm s^{-1}), the speed changed in the range of -2 to -14 cm s^{-1}, with a corresponding standard deviation of approximately 2 cm s^{-1}. The mean speed and the standard deviation are summarised in table 2 for all of the cases. The current fluctuations tend to increase with the mean speed. However, the standard deviation is smaller in the case of coflowing current, as one can see by comparing cases 5 (-7.79 cm s^{-1}) and 6 (7.41 cm s^{-1}). This is because the inlet and outlet configuration of the current circulation system is such that the coflowing condition is better regulated.

https://doi.org/10.1017/jfm.2015.578 Published online by Cambridge University Press

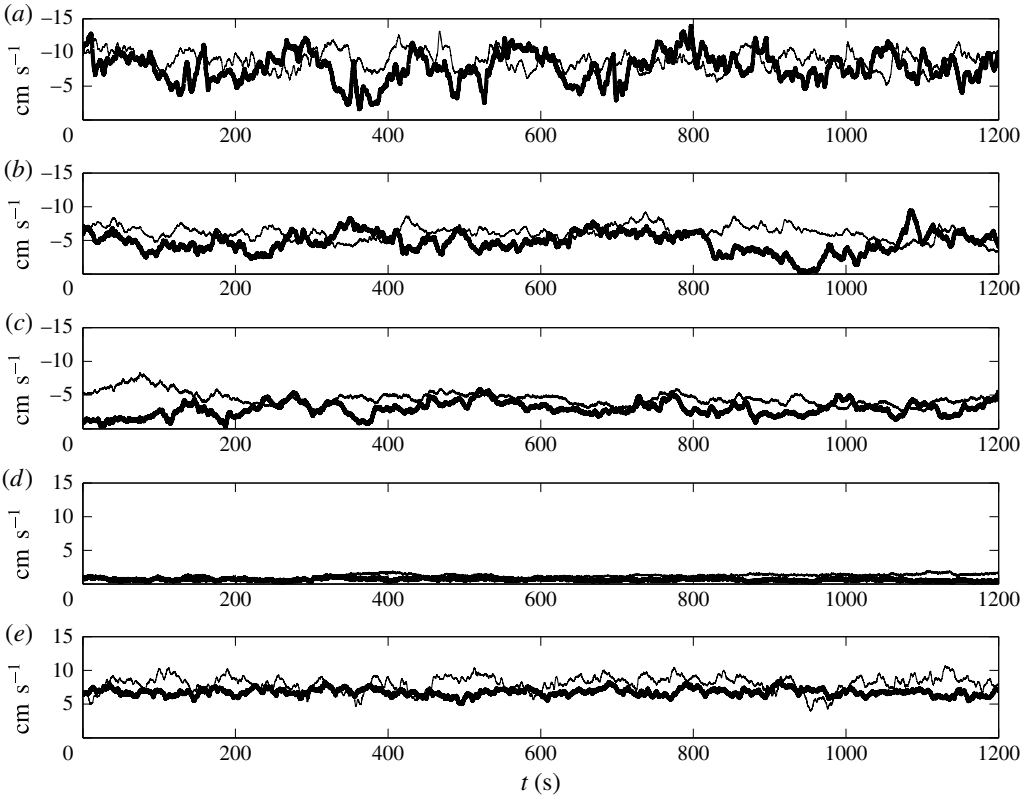

FIGURE 2. Current speeds for (*a*) case 5, −7.79 cm s^{-1}; (*b*) case 6, −5.39 cm s^{-1}; (*c*) case 7, −3.71 cm s^{-1}; (*d*) case 8, +0.89 cm s^{-1} and (*e*) case 9, +7.41 cm s^{-1}. The thick solid line is for measurement at 20 m and the thin solid line is at 10 m. The mean quantities are listed in table 2.

4. Results: third-order resonant wave interaction experiments

4.1. *Third-order resonance in a narrow channel*

4.1.1. *Tertiary wave interaction (cases* 1 *and* 2*)*

The classical experiments of Longuet-Higgins & Smith (1966) and McGoldrick *et al.* (1966) are revisited. Unlike the experiments conducted in a square basin with two wavemakers generating primary and secondary waves propagating normal to each other, the primary wave (2.2 m, $f_1 = 0.84$ Hz) and the tertiary waves (1.09 m, $f_3 = 1.20$ Hz) propagating at an angle of 9.4° were generated by the directional wavemaker (case 1, figure 3*a*). The secondary wave at a frequency of $f_2 = 2f_1 - f_3 = 0.484$ Hz should grow in the case of exact resonance. The corresponding wavelength is 6.67 m, which is 2/3 of the tank width. Because the secondary wave propagates across the tank, it will inevitably excite a sloshing mode in the tank (Jones 1984; Kit *et al.* 1987; Yao *et al.* 1994). By intentionally exciting this cross-wave, the detection of the third-order wave resonance should become easy (case 1, figure 3*a*). For comparison, the oblique wave angle of f_3 was changed to 20° which greatly deviates from the resonance condition (case 2, figure 3*b*). As expected, the energy level of f_2 in the resonant case is much higher than that of the off-resonant case. This substantiates that four-wave interaction can occur in a narrow basin if the wave

https://doi.org/10.1017/jfm.2015.578 Published online by Cambridge University Press

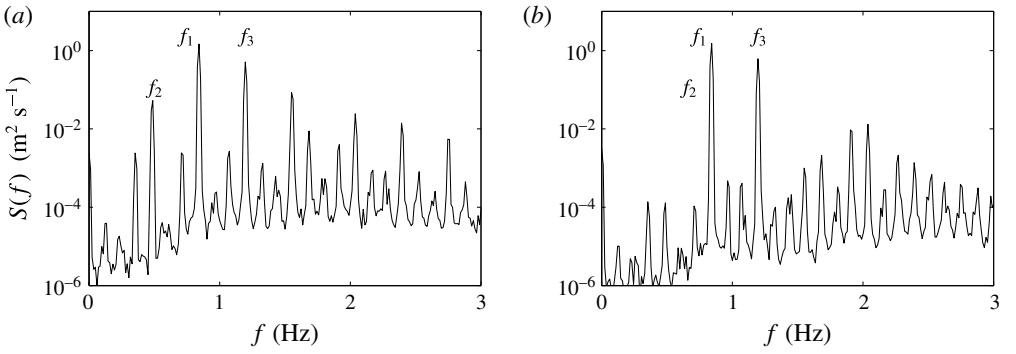

FIGURE 3. Spectrum at 30 m for the exact resonant case (*a*) and an off-resonant case (*b*). The frequency resolution is 0.122 Hz and the number of degrees of freedom is approximately 20. A Hamming window was applied.

	20 m				10 m				Mean			
Case	$\overline{U}$	$\overline{u'^2}$	$(\overline{u'^2})^{0.5}$	T.i.	$\overline{U}$	$\overline{u'^2}$	$(\overline{u'^2})^{0.5}$	T.i.	$\overline{U}$	$\overline{u'^2}$	$(\overline{u'^2})^{0.5}$	T.i.
5	−7.79	4.72	2.17	0.28	−8.85	2.00	1.41	0.16	−8.32	3.36	1.83	0.22
6	−4.68	2.38	1.54	0.33	−6.11	1.07	1.03	0.17	−5.39	1.73	1.31	0.24
7	−2.93	1.09	1.04	0.36	−4.48	0.97	0.98	0.22	−3.71	1.03	1.01	0.27
8	6.77	0.27	0.52	0.08	8.05	1.29	1.13	0.14	7.41	0.78	0.88	0.12
9	0.65	0.03	0.17	0.27	1.13	0.12	0.35	0.31	0.89	0.07	0.27	0.31

TABLE 2. Current conditions for cases 5–9. The mean $\overline{U}$, the variance $\overline{u'^2}$, the standard deviation $\sigma = (\overline{u'^2})^{0.5}$ and the turbulence intensity $\sigma/\overline{U}$ of the current are estimated from measurements at 10 and 20 m from the wavemaker. The means of these are shown as well.

parameters are selected appropriately. However, the result of this experiment cannot be compared with the theoretical growth rate, because the cross-wave does not grow in time or fetch. It is a standing wave triggered by the resonant wave interaction.

4.1.2. *Discrete interaction approximation quadruplet interaction (cases* 3 *and* 4*)*

The DIA (Hasselmann & Hasselmann 1985) is widely used in operational wave modelling. The three waves that satisfy the resonance condition (3.2*a*–*c*) are considered to have the largest contribution to the kinetic integral of Hasselmann (1962) among all the other quartets. At approximately 30 wavelengths from the wavemaker (20 m fetch), spectra with distinct peaks develop. A peak around 1.64 Hz appears in both resonant (figure 4*a*,*b*) and off-resonant (figure 4*c*,*d*) cases, but their energy levels differ significantly. The magnitude of the tertiary wave at 1.64 Hz is an order of magnitude smaller in the off-resonant case than in the exact resonant one. For resonant conditions, the tertiary wave grows to approximately 25 % of the primary wave at 1.3 Hz (figure 4*b*). The spectral peaks at high frequencies (figure 4*a*,*c*) do not seem to differ in magnitude. It is conjectured that these waves, including the 1.64 Hz wave of the off-resonant case, are bound harmonics.

The normalised tertiary wave amplitude (f_3, figure 5*a*) grows linearly in the first 10 m or 16 wavelengths from the wavemaker. In the case of exact resonance (black

https://doi.org/10.1017/jfm.2015.578 Published online by Cambridge University Press

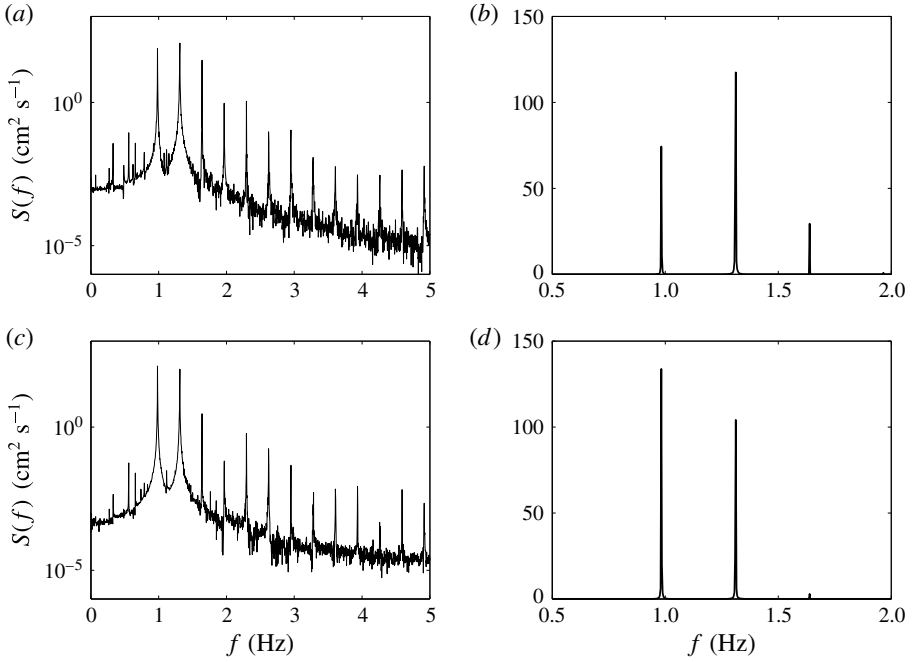

FIGURE 4. Spectrum at 20 m of the exact resonant case (*a*,*b*) and the off-resonant case (*c*,*d*) of the DIA near-resonance experiment. The frequency resolution is 0.0031 Hz and the number of degrees of freedom is 4. No window function is used.

circles, figure 5*a*), the amplitude grows more or less in accord with the growth rate estimated by potential theory (see § 2). The solid line corresponds to the linear growth curve estimated from (2.12*a*). The growth rate was estimated using the observed wave amplitude and was doubled to take into consideration the two quartet systems with secondary waves propagating obliquely at $\pm 33.6°$. A good agreement is found for the first 16 wavelengths. Gradually the growth slows down and stops; a slight signature of declination is seen towards the end of the tank (at approximately 40 m fetch or 60 wavelengths). On the contrary, the tertiary wave amplitude remains unchanged for the off-resonant case (open circles, figure 5*a*).

4.2. *Discrete interaction approximation cases with current (cases* 5–9*)*

The exact and the off-resonant cases of the DIA quartet as described in the previous section will serve as benchmarks for the four-wave interaction experiment under the influence of current. The wavemaker signal was kept the same (0.91 m primary wave at 0° and 1.6 m secondary wave at $-33.6°$) for the opposing (-8.32, -5.39 and -3.71 cm s^{-1}) and the coflowing (7.41 and 0.89 cm s^{-1}) current cases. The energy of the tertiary wave E was extracted from the wave spectrum (e.g. figure 4), and its normalised amplitude E/E_0, where E_0 is the total energy, is plotted against distance from the wavemaker in figure 5. The opposing current cases are summarised in figure 5(*b*). Compared with the benchmark case (exact resonance without current, solid circle), the growth of the tertiary wave saturates at a shorter fetch and the energy remains smaller for cases with current. As the opposing current speed becomes larger, the energy tends to saturate at a much shorter fetch (solid square,

https://doi.org/10.1017/jfm.2015.578 Published online by Cambridge University Press

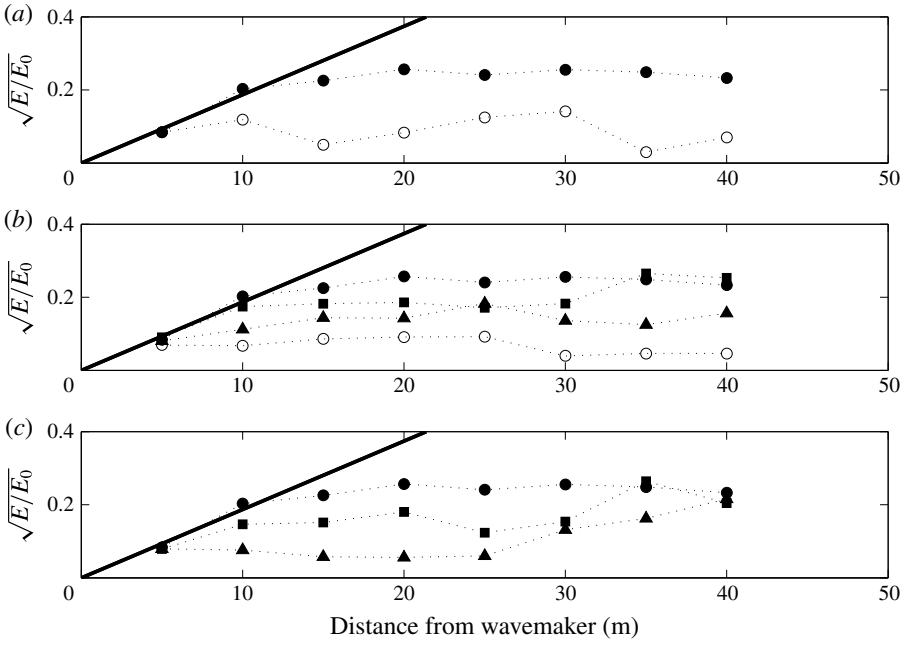

FIGURE 5. Amplitudes of the tertiary waves of the DIA combinations. (*a*) Solid circles, resonant case; open circles, off-resonant case. (*b*) Resonant cases with opposing currents: solid circles, 0 cm s^{-1}; solid squares, with -3.71 cm s^{-1}; solid triangles, with -5.39 cm s^{-1}; open circles, -8.32 cm s^{-1}. (*c*) Resonant cases with coflowing currents: solid circles, 0 cm s^{-1}; solid squares, with 0.89 cm s^{-1}; solid triangles, with 7.41 cm s^{-1}.

case 7, -3.71 cm s^{-1}; solid triangle, case 6, -5.39 cm s^{-1}; open circle, case 5, -8.32 cm s^{-1}). In fact, at -8.32 cm s^{-1}, the evolution is somewhat like the off-resonant case shown in figure 5 (see the open circles in *a*). Therefore, it is conjectured that the four-wave resonance is impaired because of the opposing current. On the other hand, the four-wave resonance may be impaired for the coflowing current case as well (figure 5*c*). As the current speed increases, the energy of the tertiary wave reduces; for the 7.41 cm s^{-1} case, case 8, the evolution resembles the off-resonant case, case 4.

Why does the four-wave resonance deteriorate under the influence of current? Let us first consider the effect of the Doppler shift, $\sigma = \omega + \boldsymbol{k}\cdot\boldsymbol{U}$. The Doppler shifts of all of the waves will accumulate in the detuning term of the frequency resonance condition (2.3). When the Doppler velocity is constant for all of the waves, the resonance detuning will nullify because of the exact wavenumber resonance condition, $\Delta_{kU} = (\boldsymbol{k}_1 + \boldsymbol{k}_2 - \boldsymbol{k}_3 - \boldsymbol{k}_4)\cdot\boldsymbol{U} = 0$. This is not always the case since the Doppler velocity may depend on the wavenumber (e.g. Stewart & Joy 1974),

$$\boldsymbol{U}_i = k_i \int_{-\infty}^{0} \boldsymbol{U}(z)\exp(k_i z)\,\mathrm{d}z, \quad \text{where } i = 1, 2, 3, 4. \tag{4.1}$$

The velocity field in the tank has a vertical shear, figure 1(*c*) and Toffoli *et al.* (2013), and therefore the effective Doppler velocity depends on the wavenumber $\boldsymbol{U}_i(\boldsymbol{k}_i)$. As a result, the shift in frequencies due to current will accumulate in the resonance detuning term,

$$\Delta_{kU} = \boldsymbol{k}_1\cdot\boldsymbol{U}_1 + \boldsymbol{k}_2\cdot\boldsymbol{U}_2 - \boldsymbol{k}_3\cdot\boldsymbol{U}_3 - \boldsymbol{k}_4\cdot\boldsymbol{U}_4 \neq 0. \tag{4.2}$$

https://doi.org/10.1017/jfm.2015.578 Published online by Cambridge University Press

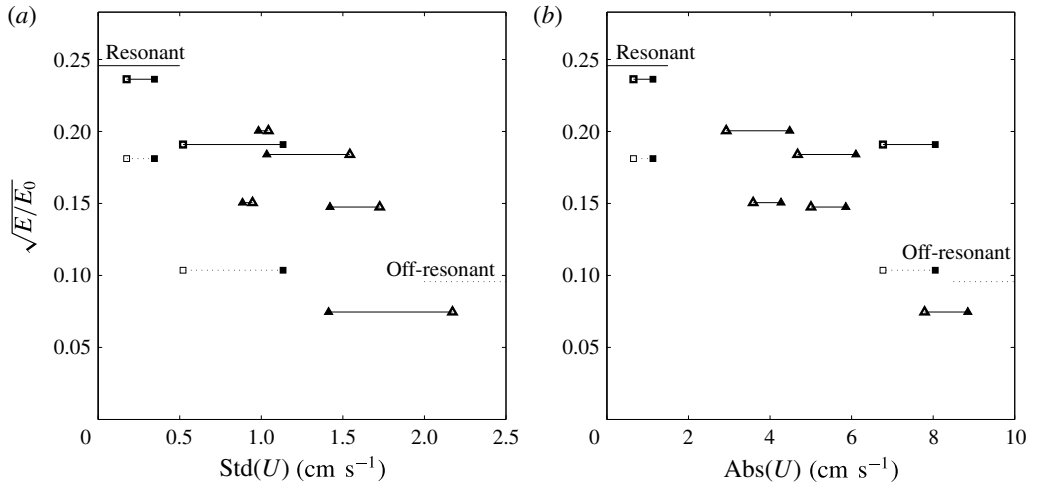

FIGURE 6. Amplitude of the tertiary waves compared with (*a*) the mean current speed and (*b*) the standard deviation of the current field. The open symbols denote measurements at 10 m fetch and the closed symbols denote measurements at 20 m fetch.

The resonance condition can be shifted due to horizontal velocity shear as well. The wavenumber is no longer a constant and will change in space and time. As a result of refraction $\mathrm{d}\boldsymbol{k}_i/\mathrm{d}t = -\boldsymbol{\nabla}(\boldsymbol{k}_i \cdot \boldsymbol{U}_i(x, y))$, where $i = 1, 2, 3, 4$, the exact resonance condition of the wavenumber is perturbed,

$$[\boldsymbol{k}_1 + \boldsymbol{k}_2 - \boldsymbol{k}_3 - \boldsymbol{k}_4]_{t=t_1} = \int_{t_0}^{t_1} \boldsymbol{\nabla} \Delta_{kU} \, \mathrm{d}t. \tag{4.3}$$

The effects of Doppler shift and refraction given in (4.2) and (4.3) do not explicitly depend on time. However, the temporal variation of the current speed is not negligible, as can be seen from the time series (figure 2). The standard deviation of the current speed is approximately a quarter of the mean current speed in the case of the opposing current and is approximately an eighth in the case of the coflowing current (table 2). The temporal variation is probably associated with advection of eddies in the tank, with both the vertical and horizontal changing velocity gradient over time. Bearing this in mind, the amplitude of the tertiary wave will be compared with the mean and the standard deviation of the current speed.

The normalised amplitude of the tertiary wave $(E/E_0)^{1/2}$ is compared with the mean current speed (figure 6*a*) and the standard deviation of the current speed (figure 6*b*). For the exact resonant case, E/E_0 is approximately 0.25 and is marked by a horizontal line in figure 6. The off-resonant case is also marked by a horizontal line and is approximately $E/E_0 = 0.1$. The normalised amplitudes of cases with current (solid line, opposing; dashed line, following) tend to decrease with both current speed and current variation, and at first sight it is not apparent which of the two is responsible for the suppression of the four-wave interaction. Since the standard deviation of the current speed and the mean current speed are linearly correlated (table 2), the causes of the suppression of resonant interaction cannot be inferred just from the scatter diagrams shown in figure 6.

Let us consider a steady current field so that the effect of Doppler shift introduces a constant frequency mismatch to the resonance condition (2.3). Then, the magnitude

https://doi.org/10.1017/jfm.2015.578 Published online by Cambridge University Press

	k_x	k_y	k	$ak_{initial}$
Wave 1	6.808	0	6.808	0.008
Wave 2	3.191	2.12	3.83	0.0056
Wave 3	10.425	−2.12	10.638	0

TABLE 3. The combinations of waves used for the numerical simulation. The wavenumber satisfies the exact resonance condition, i.e. $2k_{x1} = k_{x2} + k_{x3}$ and $2k_{y1} = k_{y2} + k_{y3}$.

of the nonlinear growth periodically changes on a time scale inversely proportional to Δ_{kU}, see (2.5*a*). Hence, the evolution of the tertiary wave is expected to grow and decay recursively in time. On the contrary, the observed growth of the tertiary wave under the influence of current saturates but maintains its magnitude (figure 5). We can then deduce that the effect of the current is intermittent, and, therefore, the resonance detuning is randomly changing in time. This bold hypothesis will be tested numerically in the next section.

5. Discussion

5.1. *Numerical simulation*

As a result of wave refraction and Doppler shift due to background opposing and coflowing mean current with large temporal and spatial variations, the exact resonance condition may be perturbed, (4.2) and (4.3). From the experimental results, we have inferred that the effect of a background current field is to detune the resonance condition randomly. First, we will test this hypothesis numerically, and then we will study the effect of mean current alone.

The reduced gravity equation (2.2) is solved for the exact resonance condition corresponding to the DIA quartet (appendix A). For the given set of waves (table 3), the resonance detuning due to frequency mismatch Δ_{1234} is zero, and, therefore, only the detuning due to the current effect remains.

To take into consideration the modification of the first-order dispersion relationship in potential theory, the current field needs to be a potential flow as well; e.g. Madsen & Fuhrman (2006). Therefore, the inclusion of a wavenumber-dependent Doppler effect due to rotational flows violates the framework of Zakharov's equation. However, when $U/Cg \ll 1$, the effect of vertical velocity shear can be incorporated (e.g. Qingpu 1996; Mei, Stiassnie & Yue 2005), and, as a result, the interaction coefficient is modified. In this case, through the change of Θ_{1234}, Δ_{1234} is perturbed, but Δ_{kU} remains zero as the first-order dispersion relationship is not altered. It is beyond the scope of this study to pin down whether the Δ_{1234} or Δ_{kU} is perturbed, but numerically they are equivalent (A 3), and their effects can be combined as a perturbation to the resonance detuning term.

The following resonance detuning due to current variation was introduced:

$$\Delta_{kU} = r \times 2\pi \times \text{rand}\,(-1 \sim 1), \tag{5.1}$$

where the constant r was set to be 0, 0.01, 0.02, 0.03, 0.05 and 0.1, and rand $(-1 \sim 1)$ is a real number selected randomly from a uniform distribution at each integration time step.

With no random detuning (corresponding to a case with $r = 0$), the third wave will grow linearly due to exact resonance and eventually start to influence the other waves as its amplitude becomes finite. Since the evolution is solved numerically

https://doi.org/10.1017/jfm.2015.578 Published online by Cambridge University Press

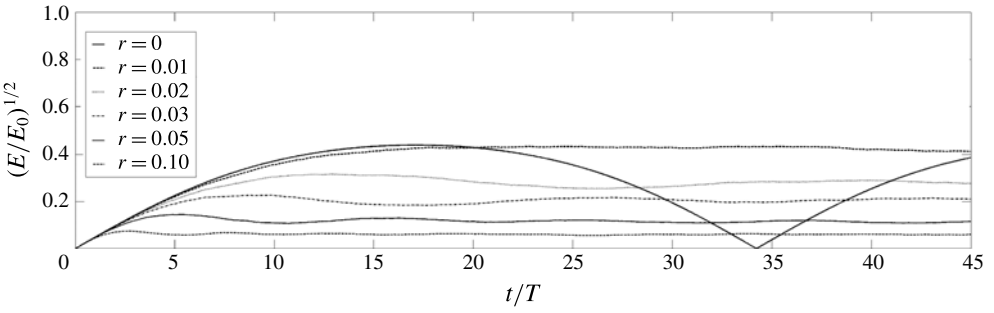

FIGURE 7. Evolution of the amplitude of the initially non-existing member of the DIA quartet numerically estimated by solving Zakharov's equation. The solid line corresponds to exact resonant interaction whereas the other lines correspond to cases with randomly perturbed resonance detuning parameters for $r = 0.01, 0.02, 0.03, 0.05$ and 0.1.

restricting the active free waves to only three DIA quartets, the amplitude of the third wave tends to go through a recurrent cycle of growth and seizure (figure 7). As the random resonance detuning is introduced, the growth of the third wave tends to slow down after some wave cycles, and eventually stops growing, subsequently maintaining its amplitude. The time scale on which the growth tends to deviate from the exact resonance case shortens with increased degree of randomness. The random resonance detuning seems to control the eventual amplitude of the third wave as well. Qualitatively, the tendency for the suppression of resonance growth is quite similar to the experimental result (figure 5), and therefore it substantiates the hypothesis that the effect of random current field annuls the resonant interaction through resonance detuning.

To rule out the possible effect of the mean current alone, additional numerical experiments were conducted imposing a constant resonance detuning:

$$\Delta_{kU} = \operatorname{sgn} C_{kU} \begin{cases} \operatorname{sgn} = -1 \text{ corresponding to } T_{1123}, \\ \operatorname{sgn} = 1 \text{ corresponding to } T_{2311}, \end{cases} \tag{5.2}$$

for $C_{kU} = -0.05, 0.01, 0.05, 0.10$. It should be noted that the values are much larger than the actual Δ_{kU} values that were estimated based on the observed vertical current shear shown in figure 1 using (4.1). The estimated values are listed in table 1. For positive C_{kU}, the growth of the initially non-existing member of the DIA quartet gradually decelerates and eventually diminishes at an earlier timing than the exact resonance case, figure 8. Then, it starts to grow again and the cycle repeats. The repetition cycle becomes shorter as the effect of constant background current C_{kU} increases. On the other hand, when C_{kU} is negative, the effect of resonance detuning is to annul the reduction of growth due to phaseshift of each member, and therefore the amplitude of the initially non-existing member becomes larger than in the exact resonance case. The tendency is distinct from the experimental results, as these did not show difference between the opposing and the coflowing mean current. Therefore, it is conjectured that the effect of random current variation is more dominant than the effect of mean background current. This conclusion, however, will not rule out the possibility of their combined effect.

The result of the random detuning is equivalent to the ensemble averaged solution of Zakharov's equation for a resonant quartet by Stiassnie & Shemer (2005). They

https://doi.org/10.1017/jfm.2015.578 Published online by Cambridge University Press

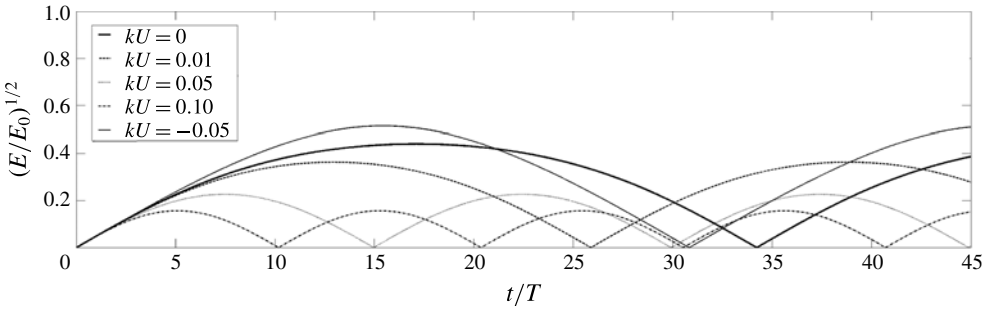

FIGURE 8. Evolution of the amplitude of the initially non-existing member of the DIA quartet numerically estimated by solving Zakharov's equation. The solid line corresponds to exact resonant interaction whereas the other lines correspond to cases with constant resonance detuning parameters for $C_{kU} = -0.05, 0.01, 0.05, 0.10$.

constructed an ensemble of deterministic simulations with random initial phases and showed that, upon averaging, the growth of the wave amplitude diminished. In our study, instead of ensemble averaging the numerous realisations, the phases were randomly perturbed and hence as the waves propagated down the tank, the current effectively prohibited the resonant interaction. Annenkov & Shrira (2006) elaborated further the findings by Stiassnie & Shemer (2005) and showed that when quasi-resonant or non-resonant interaction is taken into account, the discrepancy between Hasselman's kinetic equation and the dynamic solution by Stiassnie & Shemer (2005) is resolved. Numerous recent works have implied the significance of the dynamical time scale when the spectrum is abruptly altered by external forcing. It is of interest to see how the random current field affects the evolution of the random directional wave field in the tank, as the tank waves represent well the evolution of the spectrum on dynamic time scales.

5.2. *Evolution of irregular waves under the influence of current*

Recent works suggest that the quasi-resonant interaction plays an important role in the rapid development of Hasselman-like nonlinear energy transfer around the spectral peak on a dynamic time scale (Tanaka 2001; Pushkarev, Resio & Zakharov 2003). On the other hand, for an equilibrium spectral tail to develop, a kinetic time scale is necessary (Annenkov & Shrira 2006). However, if the energetic part of the spectrum is perturbed in time, it is plausible to think that the complete development of the spectral tail is inhibited. We, therefore, looked into the impact of the current field on the spectral tail. A random directional wave field was generated with the directional wavemaker for the JONSWAP frequency spectrum ($\gamma = 3.0$) and a fixed directional spread ($G(\theta) \propto \cos^{10}\theta$). The JONSWAP spectrum is given as $S(f) = \alpha g^2 f^{-5} \exp\{-5/4(f/f_p)^{-4}\}\gamma^{\exp\{((f-f_p)^2)/(2\sigma^2 f_p^2)\}}$, where $\sigma = 0.08$ and $\gamma = 3.0$. The α and f_p were selected such that the significant wave height was 3.5 cm and the peak period was 0.8 s. The directional spreading is given as $G(\theta) = G' \cos^{10}\theta$, where G' is a normalisation factor and θ is the wave direction. It should be noted that because of the limitation of the wavemaker, the directional spreading $G(\theta)$ was set to 0 for $|\theta| > \pi/2$, and the G' was adjusted accordingly so that the integral of G was 1. According to earlier studies (by, e.g., Waseda *et al.* 2009), despite the tank length being only of the order of 40 wavelengths, a spectral tail develops beyond 2.5 Hz,

https://doi.org/10.1017/jfm.2015.578 Published online by Cambridge University Press

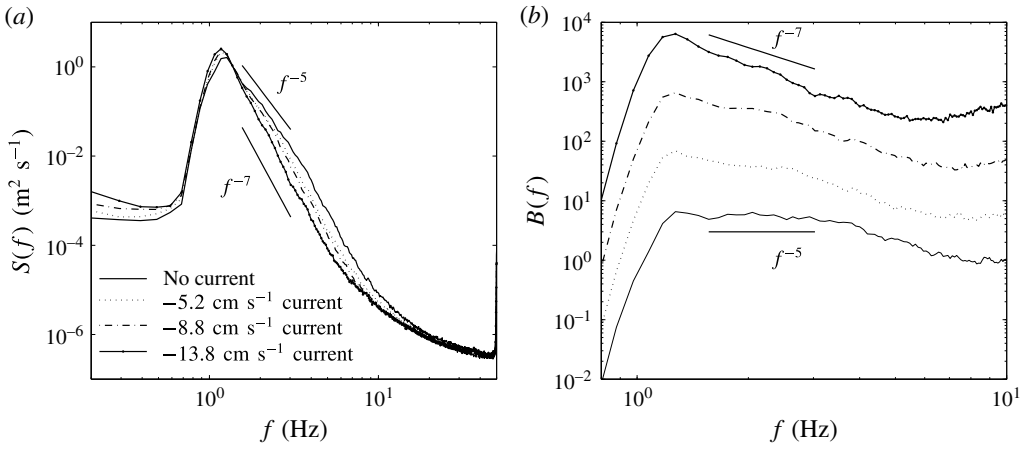

FIGURE 9. Frequency spectra of irregular directional random waves without current and with opposing current, −5.2, −8.8 and −13.8 cm s^{-1}. The unperturbed spectrum is JONSWAP with a directional spread of $G(\theta) \propto \cos^{10}\theta$. The frequency resolution is 0.0977 Hz and the number of degrees of freedom is approximately 700. A Hamming window was used. The saturated spectra $B(f) = S(f) \times f^5$ are plotted in (*b*). The lines corresponding to f^{-5} and f^{-7} are plotted for visual guidance of the slope, also indicating the range of frequency that was used to estimate the exponent of $f^{-\nu}$.

which is the upper limit of the wavemaker. They have shown that as the directional spectrum narrows, the slope of the spectral tail steepens. Under the influence of the current, the slope of the spectral tail seems to steepen as well. In figure 9, spectra with and without current at 40 m from the wavemaker are compared. The difference in the spectral tail is much larger than the effect of Doppler shift. As the mean current speed increases, the spectral tail tends to steepen (figure 9). The saturated spectra, $B(f) \equiv S(f) \times f^5$, are shown as well, in (*b*). The spectral tail tends to saturate for the case without current, but clearly deviates from saturation as the background current speed increases. The slope of the spectral tail was estimated to be between 1.56 and 3.03 Hz, indicated by the solid lines in the figures, for the cases with averaged current speeds of −13.8, −8.8, −5.2 and 0 cm s^{-1}. The exponents ν of $\omega^{-\nu}$ are 5.1, 5.8, 6.4 and 7.5 respectively. Following the corollary of § 5.1, the steepening of the spectral tail is conjectured to be a result of the resonance detuning of the four-wave interaction due to the random current field. Whether the influence of random forcing prevails on a longer time scale or not is beyond the scope of this study, and it is of interest to find out how the spectral tail further develops on the kinetic time scale.

5.3. *High-frequency spectral peaks and tail*

The special cases of the exact resonant quartet studied in this paper satisfy $2\omega_1 = \omega_2 + \omega_3$ and $2\boldsymbol{k}_1 = \boldsymbol{k}_2 + \boldsymbol{k}_3$. In the frequency domain, numerous other spectral peaks appear at higher frequencies (figures 3 and 4). These peaks may indicate either the bound harmonics or the free waves generated due to dynamical cascade (Kartashova 2009; Kartashova & Shugan 2011; Hirobe 2013). Bound harmonics may appear at the frequencies of combinations of the three waves, $n\omega_1 + m\omega_2 + l\omega_3$, where n, m and l are arbitrary integers $\ldots -2, -1, 0, 1, 2 \ldots$. Free waves may also appear due to dynamical cascading at similar frequencies to the bound harmonics. It should be noted also that

https://doi.org/10.1017/jfm.2015.578 Published online by Cambridge University Press

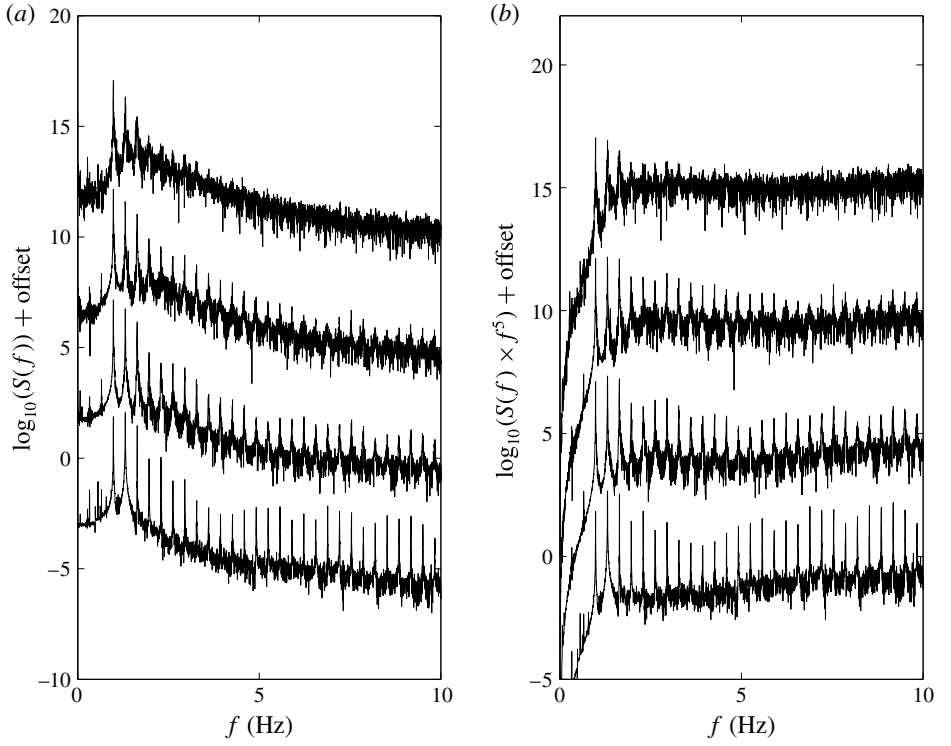

FIGURE 10. The spectral evolution for the cases without current and with opposing currents at 2, 4 and 6 cm s^{-1}, from bottom to top. The spectra were estimated from the averaged periodograms of frequency resolution 0.0031 Hz, four degrees of freedom with boxcar window function of width 327.68 s. Log–linear plots of the spectra (cm^2 s) are shown in (*a*) and log–linear plots of the saturated spectra (cm^3 s^{-4}) are shown in (*b*).

non-resonant free waves can be generated as a result of quasi-resonant interaction (e.g. Waseda *et al.* 2009).

It is apparent from the observed spectrum (figure 4) that these spectral peaks appear for cases with both resonant and off-resonant initial conditions. Just from the frequency spectrum it is not possible to distinguish whether these high-frequency peaks are free waves or not. What is notable is that the magnitude of these peaks tends to decrease for the initially off-resonant case (see the high-frequency components in figure 4). Kartashova (2009) showed that, due to interaction, a set of the resonant quartet can cascade to another resonant quartet under certain conditions. The quasi-resonant interaction can play a role in the dynamical cascade as well and thereby increases the possibility of dynamical cascade (Kartashova & Shugan 2011; Hirobe 2013). This could explain why the magnitudes of the high-frequency spectral peaks in the resonant case tend to be higher than in the off-resonant case.

Now, how would external forcing perturb this dynamical cascading process? The consequence of the background random current field was to perturb the dispersion relationship such that the exact resonance was randomly detuned. In that case, the cascade of energy should diminish and the spectral peaks should disappear. Spectra from selected cases are plotted in figure 10. Evidently the spectral peaks disappear as the magnitude of the current disturbance increases. We can infer from this result that

https://doi.org/10.1017/jfm.2015.578 Published online by Cambridge University Press

the generation of the high-frequency spectral peaks is firmly tied to the exact or quasi-resonance of the dominant waves. We conjecture that the numerous high-frequency peaks are probaby generated due to dynamical cascade, as proposed by Kartashova (2009).

It is also notable that as the current speed increases, the spectral energy seems to fill in the gaps between spectral peaks, and a continuous spectral tail develops (figure 10*a*). The energy level of this spectral tail increases with the current speed and eventually becomes comparable to the high-frequency spectral peaks. This tendency is not affected by the choice of the analysis method, i.e. the window function applied to the time series. The spectral tail up to approximately 10 Hz tends to saturate, as can be seen in the saturated spectrum ($S(f)f^5$) in figure 10(*b*). The idea of an equilibrium spectral tail proportional to f to the power of -5 was saluted and interred with dignity (Phillips 1985) but seems to resurrect over and over again (Tamura, Waseda & Miyazawa (2010) and references therein). In this study, with the absence of an energetic wind-wave spectrum and with only a few isolated resonant quartets, the saturated spectrum seems to develop with increasing magnitude of the random current forcing. This opens up a new arena of wave turbulence research where neither the dissipative forcing nor the wind input is important. What role an energy cascade of the Kolmogorov–Zakharov type (Badulin *et al.* 2005) plays under such conditions is an outstanding question.

6. Conclusion

Fifty years have passed since the first experimental validation of the four-wave resonance of surface gravity waves. In this study, we have revisited this important yet not fully exploited research topic and extended it to include the effect of vortical current field. The tertiary wave interaction, as a special case of the exact resonance quartet interaction, was investigated in a wave tank. The initially infinitesimal wave grew linearly in the distance, and the rate compared well with the theory. When a background current field was added, the growth slowed down, and as the current speed increased, the growth saturated. With further analysis of both opposing and coflowing current conditions, we reached the conclusion that the current variability affected the result rather than the mean current speed itself. The corollary of this analysis is to penalise the resonant detuning parameter of the four-wave resonance to model the effect of the random vortical current field. The potency of this idea was then investigated by conducting a numerical simulation of Zakharov's equation for tertiary waves with a random resonant detuning parameter. Although the actual interaction of wave and current in an enclosed basin might involve non-conservative processes, in this study it was shown that to a lowest-order approximation, the effect of advection and refraction of the surface gravity wave by the random current field can be condensed into the resonance detuning term, hence providing an account of the experimental result within the framework of potential theory. Although more work is warranted, the idea of radomising the resonance detuning gives an easy way to extend existing wave models based on potential theory to include the effect of wave–current interaction.

Acknowledgements

The first author thanks T. Hirobe, H. Tomita, W. Choi, V. Shrira and E. Kartashova for the discussion over the years it took to complete this paper. The work was supported partially by Grants-in-Aid for Scientific Research (KAKEN), Japan Society

https://doi.org/10.1017/jfm.2015.578 Published online by Cambridge University Press

for Promoting Science. L.C. was supported by the EU-funded project MyWave, Theme (SPA.2011.5-03). A.T. also acknowledges the International Science Linkages (ISL) Program of the Australian Academy of Science. The numerical solution of Zakharov's equation is based on a code developed in cooperation with O. Oshri when the first author was at the University of California, Santa Barbara.

Appendix A

Zakharov's equation (2.2) is solved numerically by introducing the canonical variable B_i, where $b_i = B_i \exp(-\mathrm{i}\omega_i t)$,

$$\mathrm{i}\frac{\partial B_0}{\partial t} = \sum_{0+1-2-3} T_{0123} B_1^* B_2 B_3 \exp(-\mathrm{i}\Delta_{0123} t). \tag{A 1}$$

The equation (A 1) is further modified for this study by replacing $B_i = c_{gi}^{1/2} A_i(\boldsymbol{k})$, where $A_i(\boldsymbol{k}) \equiv a_i \exp(\mathrm{i}\theta_i)$,

$$\mathrm{i}\frac{\partial A_0}{\partial t} = \sum_{0+1-2-3} T_{0123} \left(\frac{c_{g1} c_{g2} c_{g3}}{c_{g0}}\right)^{1/2} A_1^* A_2 A_3 \exp(-\mathrm{i}\Delta_{0123} t). \tag{A 2}$$

Combinations of the quartet that satisfy the wavenumber condition $\boldsymbol{k}_0 + \boldsymbol{k}_1 - \boldsymbol{k}_2 - \boldsymbol{k}_3 = 0$ are selected within the code, so that the coupled evolution equations for an arbitrary number of waves can be solved. Both resonant interaction terms T_{1234} and amplitude dispersion terms such as T_{1111} and T_{1212} are automatically generated. The time integration scheme is fourth-order Runge–Kutta.

To incorporate the current effect, (A 2) is modified as follows:

$$\mathrm{i}\frac{\partial A_0}{\partial t} = \sum_{0+1-2-3} T_{0123} \left(\frac{c_{g1} c_{g2} c_{g3}}{c_{g0}}\right)^{1/2} A_1^* A_2 A_3 \exp(-\mathrm{i}(\Delta_{0123} + \Delta_{kU}) t), \tag{A 3}$$

where Δ_{kU} represents the resonance detuning due to the background current field. Numerically, the Δ_{kU} was parameterised, for tertiary interaction of waves f_1, f_2 and f_3 satisfying $2\omega_1 = \omega_2 + \omega_3$, to mimic the effect of mean background current,

$$\Delta_{kU} = \mathrm{sgn}\, C_{kU} \begin{cases} \mathrm{sgn} = -1 \text{ corresponding to } T_{1123}, \\ \mathrm{sgn} = 1 \text{ corresponding to } T_{2311}, \end{cases} \tag{A 4}$$

and to mimic the effect of current variability,

$$\Delta_{kU} = r \times 2\pi \times \mathrm{rand}\,(-1 \sim 1), \tag{A 5}$$

where C_{kU} and r are arbitrary positive control parameters. The $\mathrm{rand}\,(-1 \sim 1)$ is a real number selected randomly from a uniform distribution between -1 and 1 at each integration time step.

REFERENCES

ANNENKOV, S. Y. & SHRIRA, V. I. 2006 Role of non-resonant interactions in the evolution of nonlinear random water wave fields. *J. Fluid Mech.* **561**, 181–207.

BADULIN, S. I., PUSHKAREV, A. N., RESIO, D. & ZAKHAROV, V. E. 2005 Self-similarity of wind-driven seas. *Nonlinear Process. Geophys.* **12** (6), 891–945.

https://doi.org/10.1017/jfm.2015.578 Published online by Cambridge University Press

BENNEY, D. J. 1962 Non-linear gravity wave interactions. *J. Fluid Mech.* **14** (4), 577–584.

CAVALERI, L., ALVES, J.-H. G. M., ARDHUIN, F., BABANIN, A., BANNER, M., BELIBASSAKIS, K., BENOIT, M., DONELAN, M., GROENEWEG, J., HERBERS, T. H. C., HWANG, P., JANSSEN, P. A. E. M., JANSSEN, T., LAVRENOV, I. V., MAGNE, R., MONBALIU, J., ONORATO, M., POLNIKOV, V., RESIO, D., ROGERS, W. E., SHEREMET, A., MCKEE SMITH, J., TOLMAN, H. L., VAN VLEDDER, G., WOLF, J. & YOUNG, I. 2007 Wave modelling – the state of the art. *Prog. Oceanogr.* **75** (4), 603–674.

DALRYMPLE, R. A. 1989 Directional wavemaker theory with sidewall reflection. *J. Hydraul. Res.* **27** (1), 23–34.

FUHRMAN, D. R., MADSEN, P. A. & BINGHAM, H. B. 2006 Numerical simulation of lowest-order short-crested wave instabilities. *J. Fluid Mech.* **563**, 415–441.

HAMMACK, J. L., HENDERSON, D. M. & SEGUR, H. 2005 Progressive waves with persistent two-dimensional surface patterns in deep water. *J. Fluid Mech.* **532**, 1–52.

HASSELMANN, K. 1962 On the non-linear energy transfer in a gravity-wave spectrum. *J. Fluid Mech.* **12** (15), 481–500.

HASSELMANN, S. & HASSELMANN, K. 1985 Computations and parameterizations of the nonlinear energy transfer in a gravity-wave spectrum. Part I: a new method for efficient computations of the exact nonlinear transfer integral. *J. Phys. Oceanogr.* **15** (11), 1369–1377.

HIROBE, T. 2013 Numerical study of nonlinear ineteraction of ocean waves and wind influence. PhD thesis, The University of Tokyo.

HJELMERVIK, K. B. & TRULSEN, K. 2009 Freak wave statistics on collinear currents. *J. Fluid Mech.* **637**, 267–284.

JANSSEN, P. 2004 *The Interaction of Ocean Waves and Wind*. Cambridge University Press.

JANSSEN, P. A. E. M. 2003 Nonlinear four-wave interactions and freak waves. *J. Phys. Oceanogr.* **33** (4), 863–884.

JONES, A. F. 1984 The generation of cross-waves in a long deep channel by parametric resonance. *J. Fluid Mech.* **138**, 53–74.

KARTASHOVA, E. 2009 Discrete wave turbulence. *Eur. Phys. Lett.* **87** (4), 44001.

KARTASHOVA, E. & SHUGAN, I. V. 2011 Dynamical cascade generation as a basic mechanism of Benjamin–Feir instability. *Eur. Phys. Lett.* **95** (3), 30003.

KIT, E., SHEMER, L. & MILOH, T. 1987 Experimental and theoretical investigation of nonlinear sloshing waves in a rectangular channel. *J. Fluid Mech.* **181**, 265–291.

KRASITSKII, V. P. 1994 On reduced equations in the Hamiltonian theory of weakly nonlinear surface waves. *J. Fluid Mech.* **272**, 1–20.

LIAO, S.-J. 2011 On the homotopy multiple-variable method and its applications in the interactions of nonlinear gravity waves. *Commun. Nonlinear Sci. Numer. Simul.* **16** (3), 1274–1303.

LIU, Z. & LIAO, S.-J. 2014 Steady-state resonance of multiple wave interactions in deep water. *J. Fluid Mech.* **742**, 664–700.

LIU, Z., XU, D., LI, J., PENG, T., ALSAEDI, A. & LIAO, S. J. 2015 On the existence of steady-state resonant waves in experiments. *J. Fluid Mech.* **763**, 1–23.

LONGUET-HIGGINS, M. S. 1962 Resonant interactions between two trains of gravity waves. *J. Fluid Mech.* **12** (3), 321–332.

LONGUET-HIGGINS, M. S. & SMITH, N. D. 1966 An experiment on third-order resonant wave interactions. *J. Fluid Mech.* **25** (3), 417–435.

MADSEN, P. A. & FUHRMAN, D. R. 2006 Third-order theory for bichromatic bi-directional water waves. *J. Fluid Mech.* **557**, 369–397.

MCGOLDRICK, L. F., PHILLIPS, O. M., HUANG, N. E. & HODGSON, T. H. 1966 Measurements of third-order resonant wave interactions. *J. Fluid Mech.* **25** (3), 437–456.

MEI, C. C., STIASSNIE, M. & YUE, D. K.-P. 2005 *Theory and Applications of Ocean Surface Waves: Nonlinear Aspects*, vol. 23. World Scientific.

MILES, J. W. 1957 On the generation of surface waves by shear flows. *J. Fluid Mech.* **3** (2), 185–204.

ONORATO, M., PROMENT, D. & TOFFOLI, A. 2011 Triggering rogue waves in opposing currents. *Phys. Rev. Lett.* **107** (18), 184502.

https://doi.org/10.1017/jfm.2015.578 Published online by Cambridge University Press

PHILLIPS, O. M. 1958 The equilibrium range in the spectrum of wind-generated waves. *J. Fluid Mech.* **4** (4), 426–434.

PHILLIPS, O. M. 1960 On the dynamics of unsteady gravity waves of finite amplitude. Part 1. The elementary interactions. *J. Fluid Mech.* **9** (2), 193–217.

PHILLIPS, O. M. 1985 Spectral and statistical properties of the equilibrium range in wind-generated gravity waves. *J. Fluid Mech.* **156**, 505–531.

PUSHKAREV, A., RESIO, D. & ZAKHAROV, V. 2003 Weak turbulent approach to the wind-generated gravity sea waves. *Physica* D **184** (1), 29–63.

QINGPU, Z. 1996 Nonlinear instability of wavetrain under influences of shear current with varying vorticity and air pressure. *Acta Mechanica Sin.* **12** (1), 24–38.

STEWART, R. H. & JOY, J. W. 1974 HF radio measurements of surface currents. In *Deep Sea Research and Oceanographic Abstracts*, vol. 21, pp. 1039–1049. Elsevier.

STIASSNIE, M. & SHEMER, L. 2005 On the interaction of four water-waves. *Wave Motion* **41** (4), 307–328.

TAKEZAWA, S., KOBAYASHI, K. & KASAHARA, A. 1988 Directional irregular waves generated in a long tank. *J. Soc. Naval Architects of Japan* **163** (6), 222–232.

TAMURA, H., WASEDA, T. & MIYAZAWA, Y. 2010 Impact of nonlinear energy transfer on the wave field in Pacific hindcast experiments. *J. Geophys. Res.* **115**, C12036.

TANAKA, M. 2001 Verification of Hasselmann's energy transfer among surface gravity waves by direct numerical simulations of primitive equations. *J. Fluid Mech.* **444**, 199–221.

TOFFOLI, A., WASEDA, T., HOUTANI, H., CAVALERI, L., GREAVES, D. & ONORATO, M. 2015 Rogue waves in opposing currents: an experimental study on deterministic and stochastic wave trains. *J. Fluid Mech.* **769**, 277–297.

TOFFOLI, A., WASEDA, T., HOUTANI, H., KINOSHITA, T., COLLINS, K., PROMENT, D. & ONORATO, M. 2013 Excitation of rogue waves in a variable medium: an experimental study on the interaction of water waves and currents. *Phys. Rev.* E **87** (5), 051201.

TOMITA, H. 1989 Theoretical and experimental investigations of interaction among deep-water gravity waves. PhD thesis, The University of Tokyo.

TRULSEN, K., STANSBERG, C. T. & VELARDE, M. G. 1999 Laboratory evidence of three-dimensional frequency downshift of waves in a long tank. *Phys. Fluids* **11** (1), 235–237.

TULIN, M. P. & WASEDA, T. 1999 Laboratory observations of wave group evolution, including breaking effects. *J. Fluid Mech.* **378**, 197–232.

WASEDA, T., KINOSHITA, T. & TAMURA, H. 2009 Evolution of a random directional wave and freak wave occurrence. *J. Phys. Oceanogr.* **39** (3), 621–639.

WHITE, B. S. & FORNBERG, B. 1998 On the chance of freak waves at sea. *J. Fluid Mech.* **355**, 113–138.

WU, C. H. & YAO, A. 2004 Laboratory measurements of limiting freak waves on currents. *J. Geophys. Res.* **109**, C12002.

XU, D., LIN, Z., LIAO, S. & STIASSNIE, M. 2012 On the steady-state fully resonant progressive waves in water of finite depth. *J. Fluid Mech.* **710**, 379–418.

YAO, Y., TULIN, M. P. & KOLAINI, A. R. 1994 Theoretical and experimental studies of three-dimensional wavemaking in narrow tanks, including nonlinear phenomena near resonance. *J. Fluid Mech.* **276**, 211–232.

ZAKHAROV, V. E. 1968 Stability of periodic waves of finite amplitude on the surface of a deep fluid. *J. Appl. Mech. Tech. Phys.* **9** (2), 190–194.

https://doi.org/10.1017/jfm.2015.578 Published online by Cambridge University Press